**Title:** Long-distance early endosome motility in *Aspergillus fumigatus* promotes normal hyphal growth behaviors in controlled microenvironments but is dispensable for virulence

**Running title:** Endosome motility in growth and pathogenesis

**Authors:** Baronger Dowell Bieger[1,2], Audra Mae Rogers[1], Steven Bates[3] and Martin John Egan[1,2*]
Corresponding author*

**Contact Information:**
1. Department of Entomology and Plant Pathology, University of Arkansas Systems Division of Agriculture, Fayetteville, Arkansas, 72701, USA
2. Cell and Molecular Biology program, University of Arkansas, Fayetteville, Arkansas, 72701
3. Medical Research Council Centre for Medical Mycology at the University of Exeter, Exeter, EX4 4QD, UK

**Synopsis:** Early endosomes are well-known to undergo long-distance microtubule-dependent trafficking in filamentous fungi, but the physiological importance of this phenomenon remains largely unclear. Here, we demonstrate, through targeted disruption of the FtsA/HookA/FhipA motor-cargo tethering complex, that dynein-dependent early endosome motility is dispensable for pathogenesis by the human opportunistic pathogen *Aspergillus fumigatus*, but is required for normal contact-mediated hyphal growth behaviors within controlled microenvironments.

**Abstract:**
In filamentous fungi, early endosomes are continuously trafficked to, and from, the growing hyphal tip by microtubule-based motor proteins, serving as platforms for the long-distance transport of diverse cargos including mRNA, signaling molecules, and other organelles which hitchhike on them. While the cellular machinery for early endosome motility in filamentous fungi are fairly well characterized, the broader physiological significance of this process remains less well understood. We set out to determine the importance of long-distance early endosome trafficking in *Aspergillus fumigatus*, an opportunistic human pathogenic fungus that can cause devastating pulmonary infections in immunocompromised individuals. We first characterized normal early endosome motile behavior in *A. fumigatus*, then generated a mutant in which early endosome motility is severely perturbed through targeted deletion of the gene encoding for FtsA, one of a complex of proteins that links early endosomes to their motor proteins. Using a microfluidics-based approach we show that contact-induced hyphal branching behaviors are impaired in Δ*ftsA* mutants, but that FtsA-mediated early endosome motility is dispensable for virulence in an invertebrate infection model. Overall, our study provides new insight into early endosome motility in an important human pathogenic fungus.

**Keywords:** Fungi; endosomes; dynein; kinesin; microtubule; pathogenesis; hyphae; Aspergillus; microfluidics; virulence

**Acknowledgements:**
This study was funded by a grant from the Arkansas Biosciences Institute. We thank Robert Cramer, Sourab Dhingra, Michelle Momany, and Earl Kang for *A. fumigatus* protocols and strains, and Daniel Irimia, Felix Ellett, and Alex Hopke for providing microfluidics devices and training. The authors declare no conflict of interests.

## Introduction

Filamentous fungi have emerged as model systems for dissecting microtubule-based transport in eukaryotic cells, with early endosomes, a vesicular organelle of the endocytic pathway, serving as a model cargo to aid mechanistic discovery [1-6]. Early endosomes undergo complex bidirectional motility inside highly polarized fungal cells [7] and are transported over long distances, from apex-proximal regions, to distal subapical compartments, in a continuous conveyer belt-like stream. The motor protein kinesin-3 moves early endosomes towards the fast-growing plus end of the microtubule track[ 4,8-10], while dynein, in complex with dynactin, transports them in the opposite, retrograde direction [8]. Early endosomes are physically linked to dynein/dynactin via the FtsA/HookA/FhipA complex [1-3], which, in the model basidiomycete *Ustilago maydis*, has been shown to control the recruitment of kinesin-3, to regulate their bidirectional motility [2]. While the basic machinery driving microtubule-based early endosome transport is now well-established, the broader physiological significance of their long-distance trafficking in filamentous fungi is less well understood. The extreme polarization of filamentous fungal cells means that their growing hyphal tips, which are first to perceive new environmental stimuli, are located at considerable distances from their subapical nuclei, which orchestrate adaptive morphogenetic programs [11]. Long-distance early endosome motility in filamentous fungi has been proposed to help bridge this gap and support rapid tip-to-nucleus communication [12]. Consistent with this idea, the long-distance retrograde trafficking of early endosomes, harboring a key mitogen-activated protein kinase, was recently shown to be essential for plant pathogenic development by *U. maydis*, providing the first strong evidence for a signaling role for early endosomes in filamentous fungi [13]. In addition to their role as motile signaling platforms, early endosomes are implicated in diverse transport-related roles in filamentous fungi, supporting the motility of peroxisomes [5] and other organelles [14], which can ‘hitchhike’ on them to achieve long-distance transport [15]. Early endosomes also provide a platform for the translation, assembly, and transport of heteromeric septin complexes [16,17] and contribute to the distribution of the translation machinery [18].

We set out to explore the role of long-distance early endosome motility in the biology of the filamentous fungus *Aspergillus fumigatus*, which causes a broad spectrum of opportunistic diseases in humans, including a severe and often fatal disease called invasive pulmonary aspergillosis [19]. Lung infections begin with the inhalation of airborne spores, which are ubiquitous in almost every environment on Earth. In healthy individuals, these spores are quickly cleared from the lungs by cells of the innate immune system [20,21]. However, in the immunocompromised, spores are able to geminate and form highly polarized extensions that can penetrate the lung epithelial barrier and enter the blood stream, resulting in systemic infection [22]. We were curious as to what extent long-distance early endosome motility contributes to pathogenesis by *A. fumigatus*, and more broadly, to hyphal growth behaviors during the colonization of microenvironments. In particular, we wondered whether the rapid microtubule-dependent transport of early endosomes from the hyphal tip to subapical regions contributes to the ability of *A. fumigatus* to respond appropriately to topographical and mechanical stimuli [23]. While the definitive mechanosensing machinery in filamentous fungi remain elusive [24], we reasoned that early endosomes might provide a platform for the fast retrograde propagation of contact-induced signals originating at the hyphal tip. To test these ideas, we generated an *A. fumigatus* mutant in which microtubule-based early endosome motility was severely perturbed and used a microfluidics-based approach to observe and quantify

obstacle-induced hyphal growth behaviors in these mutants with single cell resolution. Lastly, we exploited an invertebrate infection model to test the importance of long-distance early endosome motility for virulence of *A. fumigatus*. Here we summarize our findings and discuss their broader significance.

**Results and Discussion**

To image early endosomes (from here in referred to as endosomes) in *A. fumigatus*, we genetically tagged the small GTPase Rab5/RabA (Afu3g10740), ortholog of the *A. nidulans* RabA[7](AN4915), with the red fluorescent protein mKate2, at its N-terminus. As expected, early endosomes underwent long-distance bidirectional movements in the highly polarized hyphae of *A. fumigatus* (Fig. 1A). Endosomes moved towards the extending hyphal tip at an average velocity of 2.36 ± 0.03 μm/s, while the average velocity of retrograde-moving endosomes was significantly faster (P<0.0001 Unpaired t test) at 2.55 ± 0.03 μm/s (Fig. 1B,D). This finding is consistent with a recent report in *A. nidulans*, where retrograde-moving endosomes were shown on average to move faster than those moving towards the hyphal tip[25]. In contrast, the average run length, which we defined as the distance moved by an endosome before stopping or changing direction, was not significantly different towards (6.70 ± 0.42 μm) or away from the hyphal tip (7.22 ± 0.44 μm) Fig. 1C,D. Given the role of endosome motility in facilitating hyphal tip-to-nucleus communication in the plant pathogenic fungus *U. maydis* [13], we sought to investigate the motile behaviors of endosomes relative to the spatial organization of nuclei in *A. fumigatus* hyphae. To do this, we genetically tagged the *A. fumigatus* Histone H1 with the green fluorescent protein TagGFP2 and determined the average position of the first five nuclei relative to the hyphal tip (Fig. 1d). The average distance from the hyphal tip to the first nucleus in *A. fumigatus* hyphae was 10.40 ± 0.58 μm, while the second, third, fourth and fifth nuclei were 15.99 ± 0.58 μm, 21.67 ± 0.58 μm, 27.79 ± 0.90 μm and 33.60 ± 2.09 μm, respectively, making the typical distance between nuclei <6 μm (Fig. 1D). Thus, the maximum run lengths we observed were sufficient to move endosomes from the hyphal tip to beyond the average position of the fourth nucleus (Fig. 1D). Consistent with this idea, when we simultaneously imaged endosomes and nuclei in *A. fumigatus* hyphae, we observed single endosomes passing multiple nuclei (Fig. 1E). Therefore, the average tip-to-nucleus distance in *A. fumigatus* is less than half that of the phytopathogenic fungus *Ustilago maydis* [13], but comparable to its close relative, the genetic model *A. nidulans* [11].

Having characterized the motile behaviors of endosomes in wild type hyphae, we next sought to generate a mutant in which endosome motility was severely and specifically perturbed. To do this, we deleted the gene encoding for the *A. fumigatus* ortholog of the *A. nidulans* protein FtsA (Fused Toes in humans), which in complex with HookA and FHIP links EE to dynein/dyanctin for microtubule-based transportation (Fig. 2A) [2,3]. As expected, endosomes accumulated aberrantly in the hyphal tips of the *ΔftsA* mutant (Fig. 2B,C) and were largely immotile (Fig. 2D). To determine the extent to which deletion of the FtsA-encoding gene disrupts endosome motility, we counted the number of endosomes that crossed a defined region of the hyphal tip over a set period of time and defined this as endosome flux. In wild type hyphae, the flux of endosomes towards and away from the hyphal tip was identical, occurring at a rate of 11 ± 3 endosomes per 20 seconds. In the *ΔftsA* mutant this was reduced to 1 ± 1 endosomes per 20 seconds in both directions (Fig. 2E). Endosomes moving towards the hyphal tip in the genetic absence of FtsA did so at velocities comparable to those in wild type hyphae (*ΔftsA* = 2.54 ± 0.16 μm/s versus wild type = 2.36 ± 0.03 μm/s) (Fig. 2F). However, the average velocity of endosomes moving away from the hyphal tip was significantly slower (Tukey's multiple comparison test, adjusted P Value = 0.0012) in the *ΔftsA* mutant compared with those in the wild

type (*ΔftsA* = 2.11 ± 0.12 μm/s versus wild type = 2.55 ± 0.03 μm/s) (Fig. 2F). The mechanistic reasons for the decreased velocity of retrograde-moving endosomes in *ΔftsA* mutants is unclear but could be due the recruitment of fewer dyneins to these endosomes compared with those in wild type hyphae. Importantly, to confirm that the observed defects in endosome motility were due specifically to genetic deletion of FtsA, we ectopically reintroduced a copy of the FtsA-encoding gene into the *ΔftsA* mutant, which largely restored endosome motile behaviors to those of the wild type strain (Fig. 2B-F). However, the ectopic expression of FtsA in the *ΔftsA* mutant *(ΔftsA::ftsA)* resulted in increased flux of endosomes both towards and away from the hyphal tip, compared to the wild type strain (wild type = 11 ± 3 endosomes, versus *ΔftsA::ftsA* = 14 ± 4 endosomes, per 20 seconds) (Fig. 2F). Thus, as expected, the cellular machinery required for dynein-dependent endosome motility is conserved between *Aspergillus* species [3,26].

Next, we set out to investigate the extent to which endosome motility contributes to hyphal growth behaviors in controlled microenvironments. Previously, *A. fumigatus* was shown to undergo elegant evasive hyphal branching in response to physical impediment [27]. We hypothesized that retrograde early endosome motility might be important for both propagating signals arising from hyphal tip-derived mechanical cues and for spatially and temporally orchestrating the resulting evasive branching responses by *A. fumigatus*. To test this idea, we germinated spores from our wild type, *ΔftsA* and *ΔftsA::ftsA* strains in custom-fabricated microfluidics devices designed to steer the growth of individual hyphae towards, and into, crescent-shaped obstacles and quantified their behaviors and responses. We measured the time it took hyphae from each strain to successfully navigate these crescent-shaped obstacles, which we defined as their 'escape' time (Fig. 3B,C). Despite a significant decrease in hyphal growth rate within microfluidics devices (*ΔftsA* = 0.54 ± 0.14 μm/min versus wild type = 0.59 ± 0.14 14 μm/min), the *ΔftsA* mutant achieved statistically comparable escape times to that of the wild type strain (*ΔftsA* = 4.1 ± 1.4 hours versus wild type = 4.3 ± 1.6 hours), which we attribute to altered contact-induced branching patterns in the *ΔftsA* mutant (Fig. D,E). On average, the *ΔftsA* mutant produced fewer branches during the navigation of crescent-shaped obstacles compared to the wild type strain (*ΔftsA* = 1.7 ± 0.8 branches versus wild type = 2.1 ± 0.9 branches). Relatively little is understood about how branching is spatially regulated in filamentous fungi [28], due in part to an historical lack of tools to induce hyphal branching in a predictable and highly controlled manner. We propose, based on our microfluidics data, that long-distance early endosome motility contributes to the spatiotemporal orchestration of subapical branching in *A. fumigatus*. Interestingly, and in support of this idea, the microtubule-dependent movement of Rab5 early endosomes is important for both axonal [29] and dendritic [30] branching in sensory neurons, which, like filamentous fungi, are extremely polarized [31]. In *A. fumigatus*, motile early endosomes could conceivably facilitate the recruitment of key morphogenetic machinery to new branch sites [32], including the transportation of heteromeric septin complexes [17], likely important for controlled hyphal branching [33]. Next, we focused on the initial point of hyphal impact and the resulting behavior of the hyphal tip and found that contact-induced apical branching was significantly reduced in the *ΔftsA* mutant compared with the wild type (*ΔftsA* = 45 ± 10% versus wild type = 71 ± 6% SD). Importantly, the hyphal growth behaviors of the *ΔftsA::ftsA* complementation strain were restored to those of the wild type, barring the average branch number (Fig. 3E), which although increased (*ΔftsA::ftsA* = 2.0 ± 1.0 branches versus 1.7 ± 0.8 branches) remained statistically similar to the *ΔftsA* mutant. In 'type 1' responses, contact with crescent-shaped obstacles resulted in immediate branching at the hyphal apex, as well as along various points of contact (Fig. 3E). In 'type 2' responses, hyphae continued to expand at their tips upon contact, resulting in substantial subapical kinking of the hyphae, and the formation of a branch site, typically at the extreme apices of the bends (Fig. 3F). The increase in 'type 2'

responses observed in the *ΔftsA* mutant could, in principle, be explained by the impaired propagation of early endosome-mediated contact-induced signals resulting in hyphal tips that don't respond appropriately to contact. Limited evidence suggests that perturbing early endosome motility in *A. oryzae*, in this case through deletion of the HookA ortholog, results in pleiotropic disruption of the Spitzenkörper [26], a specialized vesicle-organizing center located in the hyphal apex [34]. Given the role of the Spitzenkörper in controlling hyphal growth orientation [35], it is possible that impaired Spitzenkörper morphology, if also present in our *ΔftsA* mutant, might contribute to the phenotypes described here (Fig. 3F,G). However, a more compelling explanation is that blocking dynein-dependent endosome motility, which is coupled to endosome maturation [36,37], results in impaired endocytic recycling of various plasma membrane-associated cargoes including cell wall-modifying enzymes[38] and polarity determining regulators such as Cdc42/Rho GTPases [39], therein affecting the establishment of new polarity axes in the *ΔftsA* mutant. Consistent with this idea, we found that *ΔftsA* mutants produced more lateral branches growing vegetatively on solid media than the wild type and *ΔftsA::ftsA* strains (wild type and *ΔftsA::ftsA* = $1.3 \pm 1.3$ (SD) branches per 400 μm versus *ΔftsA* = $3.2 \pm 2.3$ (SD) per 400 μm (Fig. S1A), which we take as further evidence of impaired regulation of polarity establishment and/or maintenance in the absence of FtsA-mediated early endosome motility. It is important to note that because a number of other cellular cargoes achieve motility by hitchhiking on moving endosomes [5,14], the branching defects observed in *ΔftsA* mutants cannot, without additional evidence, be attributed directly to perturbed early endosome motility. Therefore, understanding their precise role requires further investigation. Surprisingly, we found no difference in the sensitivity of *ΔftsA* mutants to cell wall- and membrane-perturbing agents, or to osmotic stress (Fig S1B).

Lastly, we sought to investigate whether perturbing early endosome motility impacts upon the virulence of *A. fumigatus*. Given the importance of long-distance early endosome motility for effector-mediated plant infection by *U. maydis* [13], we wondered whether our *ΔftsA* mutant might too be compromised in virulence. *A. fumigatus* is considered an opportunistic pathogen and therefore does not rely on effectors to modulate host physiology to the same extent as plant pathogenic fungi like *U. maydis*, which have coevolved with their hosts. However, the environment-responsive secretion of proteases and secondary metabolites play important roles in virulence by *A. fumigatus* [19,40], and we hypothesized that microtubule-dependent early endosome motility might play a role in this process. We also wondered whether the subtle differences in branching behavior of our *ΔftsA* mutant might too result in altered virulence, since *A. fumigatus* mutants with constitutive hyphal branching and polarity defects are often altered in virulence [41,42]. *A. fumigatus* was recently shown to undergo evasive hyphal branching in response to encounters with neutrophils *in vivo*, which promoted fungal survival under conditions of low neutrophil abundance but resulted in enhanced neutrophil-mediated destruction when immune cell numbers were high [27]. To test whether early endosome motility is required for virulence by *A. fumigatus*, we used the well-established *Galleria mellonella* infection model [43]. Compared with the wild type and *ΔftsA::ftsA* strain, our *ΔftsA* mutants produced slightly more compact colonies (Fig. 4A), consistent with the morphology reported for *ΔhookA* [1], *ΔftsA* and *ΔfhipA* mutants in *A. nidulans* [3], but produced a statistically similar number of spores (Fig. 4B). We isolated spores from each strain, injected a total of $1 \times 10^5$ spores into the last left proleg of *G. mellonella* larvae, and monitored them daily for survival at 37 ºC. Surprisingly, we found no difference in the virulence of the *ΔftsA* mutant compared with the wild type and *ΔftsA::ftsA* strains (Fig. 4C), and therefore early endosome motility, at least in this model, is dispensable for pathogenesis. It is possible that the injection of spores directly into *G. mellonella* larvae bypasses any requirement for early endosome-mediated processes that might contribute to virulence by

*A. fumiagtus*, and that early endosome motility plays a more important role during the penetration and colonization of lung epithelial tissue in mammalian systems. In conclusion, our study largely highlights the surprising dispensability of early endosome trafficking for pathogenesis by *A. fumigatus* and demonstrates the resilience of polarized hyphal growth to major cellular perturbation.

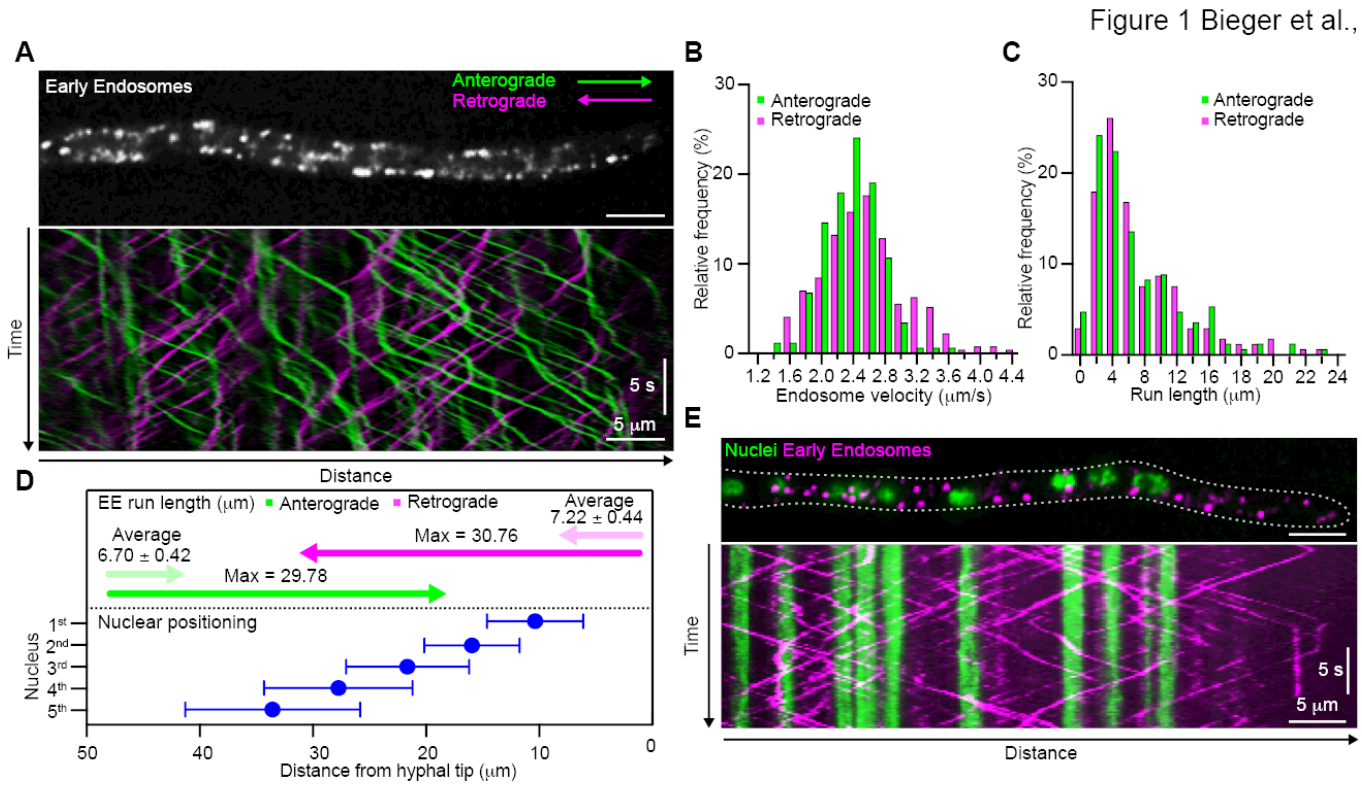


Figure 1. **Early endosomes undergo long-distance bidirectional motility in *Aspergillus fumigtaus*. A** Fluorescence micrograph showing the localization of mKate2-Rab5/RabA-labelled early endosomes in an *A. fumigatus* hypha (upper panel) and a kymograph generated from a timelapse sequence of the same hypha, showing the bidirectional trajectories of early endosomes (bottom panel). Endosome moving away from the hyphal tip (retrograde) are shown in magenta, while those moving towards the tip are shown in green. **B** Histogram of velocities of anterograde (green) and retrograde (magenta) moving endosomes in wild type hyphae. Mean velocities are 2.36 ± 0.03 μm/s (SEM) for anterograde and 2.55 ± 0.03 μm/s for retrograde moving endosomes. **C** Histogram of run lengths of anterograde (green) and retrograde (magenta) moving endosomes. For retrograde, *n* = 173 and for anterograde *n* = 170. **D** Schematic diagram depicting the average and maximum run lengths of anterograde (green arrows) and retrograde (magenta arrows) moving endosomes in wild type hyphae, relative to the average position of the first 5 nuclei (blue dots). Error bars represent SD, and *n* = 53 for each nucleus. **E** Fluorescence micrograph showing the localization of mKate2-Rab5/RabA-labelled early endosomes (magenta) and Histone H1-TagGFP2 lablled nuclei in a wild type hypha (upper panel) and a kymograph generated from a timelapse sequence of the same hypha, showing the bidirectional trajectories of early endosomes (magenta) relative to the nuclei (green).

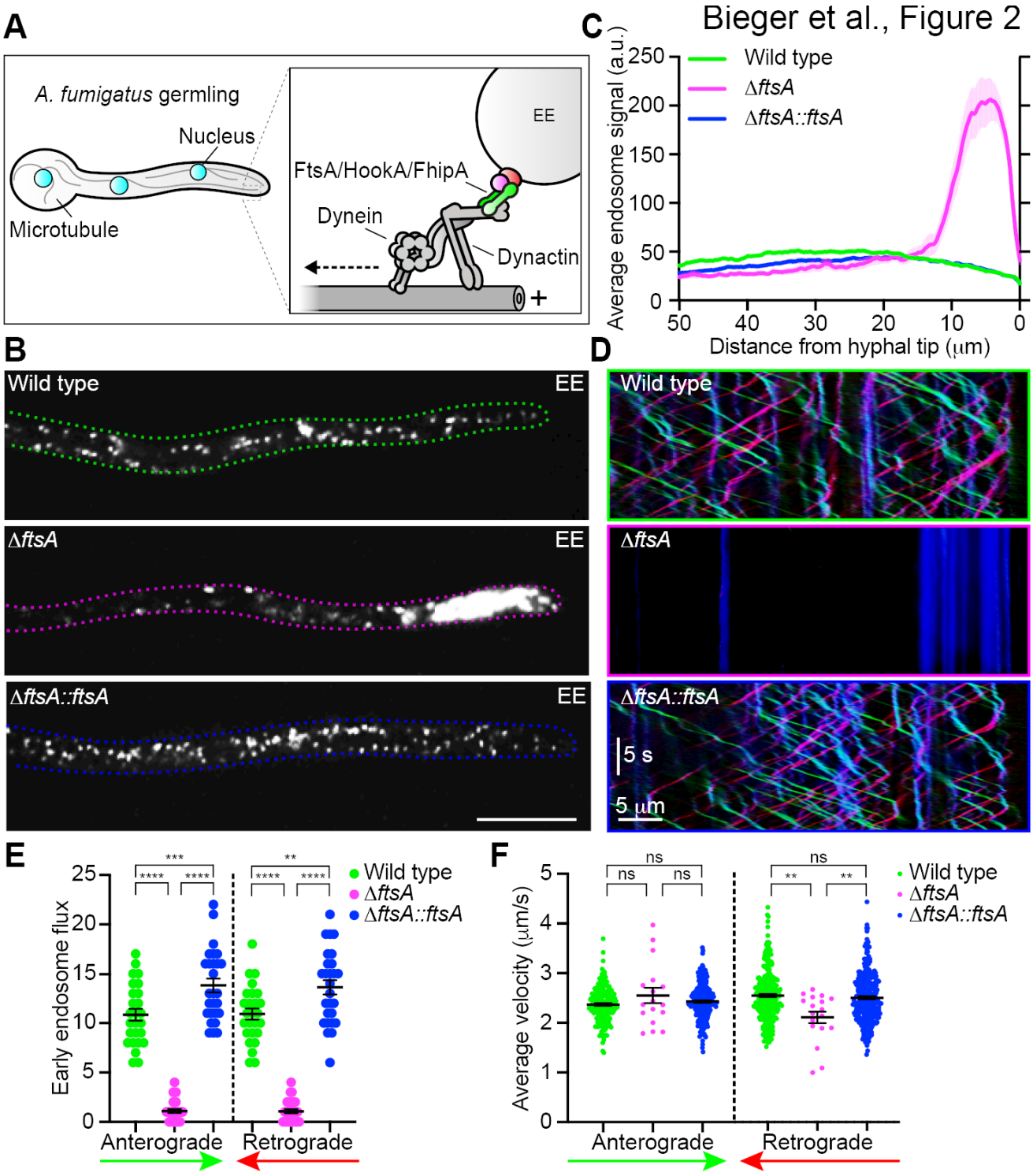


Figure 2. **FtsA is required for normal long-distance early endosome trafficking. A** Cartoon depicting the retrograde transport machinery in *A. fumigatus*, which moves early endosomes away from the hyphal tip along polarized microtubule arrays. Based on data from[3]. Early endosomes (EE) are linked to dynein/dynactin via the FtsA/HookA/FhipA complex. **B** Fluorescence micrographs showing the localization of mKate2-Rab5/RabA-labelled endosomes in wild type (top panel, green outline), Δ*ftsA* mutants (middle panel, magenta outline) and the complemented Δ*ftsA::ftsA* strain (bottom panel, blue outline). Scale = 10 μm. **C** Line scans showing the mean fluorescence intensity from mKate-Rab5/RabA-lablled endosomes in wild

type (green line), Δ*ftsA* (magenta line) and Δ*ftsA::ftsA* (blue line) strains as a function of distance from the hyphal tip. Lighter green, red and blue shading represents ± SEM. For wild type *n* = 38, for Δ*ftsA* *n* = 35, and for Δ*ftsA::ftsA* *n* = 34. **D** kymographs generated from timelapse sequences of wild type (green border), Δ*ftsA* (magenta border) and Δ*ftsA::ftsA* (blue border) hyphae showing the trajectories of mKate2-Rab5/RabA-labelled endosomes. Kymographs were filtered to show anterograde endosome trajectories in green, retrograde endosome trajectories in red, and static endosomes in blue. **E** Plots showing the flux of endosomes towards (left side) and away from (right side) the hyphal tip in wild type (green), Δ*ftsA* (magenta), and Δ*ftsA::ftsA* (blue) hyphae. **F** Plots showing the average velocity of endosomes moving towards (left side) and away from (right side) the hyphal tip in wild type (green), Δ*ftsA* (magenta), and Δ*ftsA::ftsA* (blue) hyphae. Asterisk indicate significance by one-way ANOVA with Tukey's multiple comparisons test (*p<0.05, **P<0.01, ***P<0.001, ****P<0.0001).

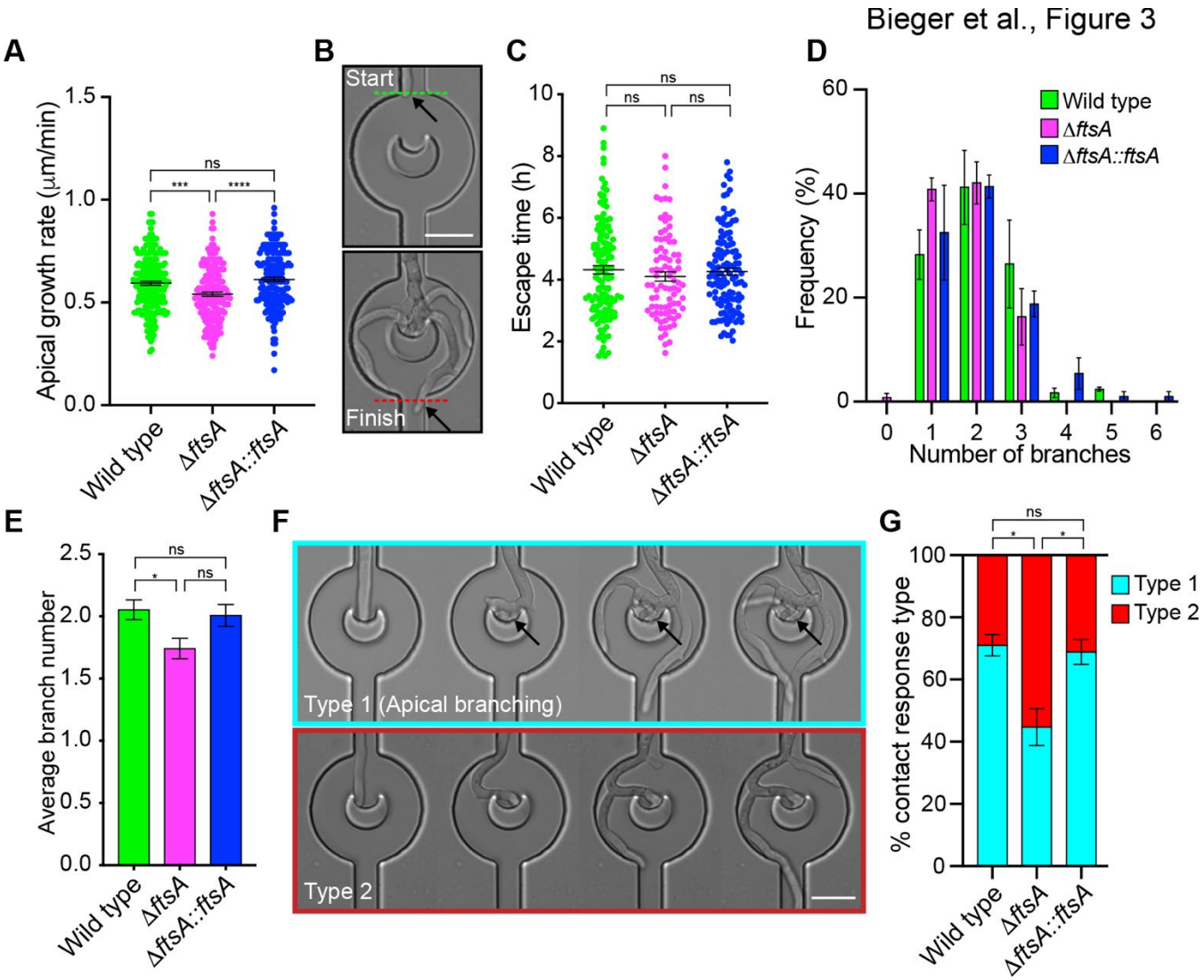


Figure 3. **Contact-induced hyphal branching behavior is altered in Δ*ftsA*. A** Plot showing the apical growth rates of wild type (green), Δ*ftsA* (magenta) and Δ*ftsA::ftsA* (blue). Mean ± SEM values are shown. For wild type, the mean hyphal velocity is 0.59 ± 0.14 μm/min (SD) and *n* = 203, for Δ*ftsA* = 0.54 ± 0.14 μm/min and *n* = 186, and for Δ*ftsA::ftsA* 0.61 ± 0.14 μm/min and *n* = 184. Asterisk indicate significance by one-way ANOVA with Tukey's multiple comparisons test (*p<0.05, **P<0.01, ***P<0.001, ****P<0.0001). **B** Micrographs demonstrating the 'escape time' metric, which represents the time taken for a given hyphal tip to extend through the red dashed line, or 'finish', having passed through the green dashed line, representing the 'start'. **C** Plot showing the escape times of wild type (green), Δ*ftsA* (magenta) and Δ*ftsA::ftsA* (blue) hyphae. Mean ± SEM values are shown. For wild type, the mean escape time is 4.3 ± 1.6 hours (SD) and *n* = 135, for Δ*ftsA* = 4.1 ± 1.4 minutes and *n* = 85, and for Δ*ftsA::ftsA* 4.3 ± 1.3 hours and *n* = 126. **D** Histogram showing the number of hyphal branches produced by the wild type (green) *n* = 132, Δ*ftsA* (magenta) *n* = 85, and Δ*ftsA::ftsA* (blue) *n* = 122. Error bars represent SEM from three independent replicates per strain. **E** Graph showing the mean number of hyphal branches produced per 'escape' for wild type (green) 2.1 ± 0.9 branches, Δ*ftsA* (magenta) 1.7 ± 0.8 branches, and Δ*ftsA::ftsA* (blue) 2.0 ± 1.0 branches. Asterisk indicate significance by one-way ANOVA with Tukey's multiple comparisons test (*p<0.05). **F** Micrographs from representative time-lapse sequences demonstrating the two major types of contact-induced hyphal responses observed. In 'type 1' responses, hyphae undergo apical branching in response to contact with

crescent-shaped obstacles, while in ‘type 2’ responses, hyphae do not undergo apical branching, and instead branches emerge subapically, likely in response to hyphal bending. **G** Graph showing the mean percentage of hyphae undergoing ‘type 1’ or ‘type 2’ responses following contact with crescent-shaped obstacles, where the cyan bar is ‘type1’ and red bar is ‘type 2’. In the wild type strain 71 ± 6% (SD) of contact-induced responses were ‘type 1’, in Δ*ftsA* 45 ± 10%, and in Δ*ftsA::ftsA* 69 ± 7%. Error bars represent ± SEM from three independent replicates per strain.

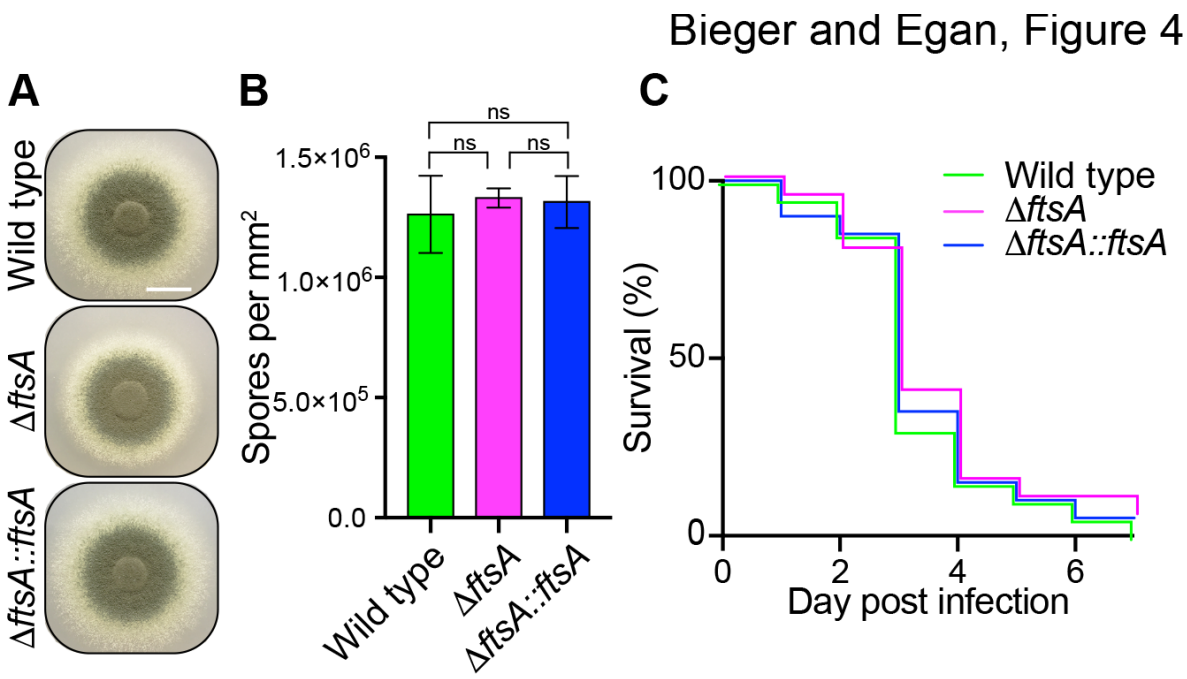


Figure 4. **Long-distance early endosome trafficking is dispensable for pathogenesis by *A. fumigatus* in an invertebrate infection model. A** Colony morphologies of the wild type, Δ*ftsA* and Δ*ftsA::ftsA* strains after 3 days growth on minimal media at 37 ºC. **B** Graph showing the average number of spores recovered per $mm^2$ from wild type (green) $1.26\times10^6 \pm 1.61\times10^5$ (SEM), Δ*ftsA* (magenta) $1.33\times10^6 \pm 4.06\times10^4$, and Δ*ftsA::ftsA* (blue) $1.31\times10^6 \pm 1.08\times10^5$ colonies. Differences were not significant (ns) by one-way ANOVA. **C** Kaplan-Meier curve showing the mean percent survival of *G. mellonella* larvae following inoculation with $1\times10^5$ spores of the wild type (green line), Δ*ftsA* (magenta line), and Δ*ftsA::ftsA* (blue line) strains. The data represent the mean values from three independent replicates, where *n* = 20 larvae per strain, per replicate. A log rank test was used for pairwise comparison among the groups, and no significant differences were identified (P>0.5 for all comparisons an replicates).

## Materials and Methods

### Strains, media, and growth conditions.

A strain of *A. fumigatus* 293 lacking functional *pyrG* and *argB* genes (AF293.6, FGSC A1138) was obtained from the Fungal Genetic Stock Center and used as an entry strain for the tagging of *rab5A* with mKate (Afu3g10740; *mKate-rabA::argB*) and the subsequent deletion of *ftsA* (Afu1g15570; *mKate-rabA::argB, ΔftsA::hyg*) and complementation (*mKate-rabA::argB, ΔftsA::hyg*, *ftsA::A. parasiticus pyrG*). To produce non-auxotrophic versions for pathogenicity testing, the uracil auxotrophy was eliminated in the *rabA* tagged and *ΔftsA* strains by inserting *A. parasiticus pyrG* at the native *pyrG* locus. The *ftsA* deletion and complementation were confirmed via diagnostic PCR. A separate *A. fumigatus* strain lacking a functional *akuB* and *pyrG* was used to generate the *rabA* (Afu3g10740) and *HH1 (*Afu3g06070) tagged strain (*mKate-rabA::hyg, HH1-GFP::ptrA*) See Table S1.1 for a full list of strains**.**

Plate cultures were grown at 37 °C on glucose minimal media (GMM) with 1% glucose. Any necessary supplements were added until strains were produced that were no longer auxotrophic. Liquid cultures for microscopy were grown in GMM with 2% glucose at 37 °C and were imaged at ambient temperatures.

All strains were generated using DNA constructs that targeted the relevant native loci as previously described [44]. Briefly, targeting regions and genes of interest were amplified from gDNA from the entry strain, while selectable markers and fluorescent protein sequences were amplified from plasmids (see Table S1.2). Fragments were assembled using yeast gap repair [45] or In-Fusion Cloning, and constructs were amplified from these plasmids for use in standard, polyethylene glycol-mediated fungal protoplast transformations, as previously described [46]. For the *ftsA* gene deletion construct, 1.0 kb upstream of the start codon and 1.0 kb downstream of the stop codon were assembled onto either end of the hyg cassette in a yeast gap repair plasmid. For the *ftsA* complementation construct, the *A. parasiticus pyrG* cassette was placed between a fragment containing 2.0 kb upstream of the start codon through the open reading frame (ORF) and the 3' untranslated region (UTR) and a fragment containing an additional 1.5 kb downstream.
To build the mKate2-RabA constructs, a 1.6 kb fragment encompassing the *rabA* promotor region was assembled upstream of the mKate2-encoding sequence, which was fused in frame with a 1.3 kb region spanning the *rabA* ORF and 3'UTR, followed by either the hygromycin cassette or *argB* marker, followed by an additional 1.0 kb of targeting sequence. For the Histone H1-TagGFP2 construct, a 1.0 kb targeting fragment encoding the end of the Histone H1 ORF was fused in frame to the TagGFP2-encoding sequence, followed by a 0.7 kb region of the Histone H1 3'UTR, the *ptrA* marker, and a 1.0 kb targeting region. Tagged transformants were screened via fluorescence microscopy and confirmed by PCR. All oligonucleotides, including those used for diagnostic PCR, can be found in Table S1.3.

### Image acquisition and analysis

Fluorescence images were collected at room temperature using a 100x 1.49 N.A oil immersion Apo TIRF Nikon objective on an inverted Nikon Ti-E Eclipse TIRF microscope equipped with Perfect Focus System (Nikon), a iXon Ultra 897 electron multiplier CCD Camera (Andor Technology), and a LUN-F laser launch equipped with 488nm (90mW), 561nm (70mW) and

405nm (50mW) lasers lines, all controlled by NIS-Elements AR (version 4.60). Data sets were deconvolved in NIS-Elements AR, with spherical aberration correction, and background subtraction, using the "Automatic" 2D deconvolution option. Images of microfluidics devices were collected at room temperature using a 20x 0.75 N.A. Plan Apo Lambda objective on the same microscope, and a Zyla 4.2 sCMOS camera (Andor Technology). Brightness and contrast adjustments to maximum intensity projections of deconvolved 2D images were made using ImageJ (version 2.0; National Institutes of Health) and Photoshop CC (2017.1.4; Adobe), and figures were compiled in Illustrator CC (22.1; Adobe).

**Automated kymograph analysis**
Directional early endosome velocities were extracted from color-coded kymographs generated from timelapse sequences using the KymographClear and KymographDirect workflows [47].

**Branching Assay**
Spores from each strain were stabbed out onto GMM and grown at 37 °C for 24 hours. The resultant colonies were cut in half and placed upside down on a 35 mm glass-bottomed FluoroDish (World Precision Instruments) for brightfield imaging with a 20X objective. The number of established branches that occurred in the first 400 µm of each hypha were counted. Branches were considered "established" when they had clearly projected themselves from source hypha. Hyphae that forked near their apical tip were measured from the longest branch.

***G. mellonella* infection assay**
Spores ($1\times10^6$) were spotted onto PDA plates and grown at 37 ºC for 5 days. Spores were then harvested in PBS+0.01% Tween-80, washed in PBS, counted on a haemocytometer and adjusted to $1\times10^7$ spores/ml in PBS. Groups of 20 wax moth larvae (UK Waxworms Ltd, Sheffield, UK), selected based on their weight (0.25-0.35g) and lack of visible melanisation, were injected with 10 µl spore suspension ($1\times10^5$ spores / larva) using a 50 µl Hamilton syringe into their last left pro-leg. Larvae were then maintained at 37 ºC in the dark, and monitored for survival daily.

**Acknowledgements:**
This study was funded by a grant from the Arkansas Biosciences Institute. We thank Robert Cramer, Sourab Dhingra, Michelle Momany, and Earl Kang for *A. fumigatus* protocols and strains, and Daniel Irimia, Felix Ellett, and Alex Hopke for providing microfluidics devices and training. The authors declare no conflict of interests.

## References


[1] J. Zhang, R. Qiu, H.N. Arst, M.A. Peñalva, X. Xiang, **HookA is a novel dynein-early endosome linker critical for cargo movement in vivo**, J. Cell Biol. 204 (2014) 1009–1026. doi:10.1083/jcb.201308009.

[2] E. Bielska, M. Schuster, Y. Roger, A. Berepiki, D.M. Soanes, N.J. Talbot, et al., **Hook is an adapter that coordinates kinesin-3 and dynein cargo attachment on early endosomes**, J. Cell Biol. 204 (2014) 989–1007. doi:10.1083/jcb.201309022.

[3] X. Yao, X. Wang, X. Xiang, **FHIP and FTS proteins are critical for dynein-mediated transport of early endosomes in *Aspergillus***, Mol. Biol. Cell. 25 (2014) 2181–2189. doi:10.1091/mbc.E14-04-0873.

[4] M.J. Egan, K. Tan, S.L. Reck-Peterson, **Lis1 is an initiation factor for dynein-driven organelle transport**, J. Cell Biol. 197 (2012) 971–982. doi:10.1083/jcb.201112101.

[5] J. Salogiannis, M.J. Egan, S.L. Reck-Peterson, **Peroxisomes move by hitchhiking on early endosomes using the novel linker protein PxdA**, J. Cell Biol. 212 (2016) 289–296. doi:10.1083/jcb.201512020.

[6] K. Tan, A.J. Roberts, M. Chonofsky, M.J. Egan, S.L. Reck-Peterson, **A microscopy-based screen employing multiplex genome sequencing identifies cargo-specific requirements for dynein velocity**, Mol. Biol. Cell. 25 (2014) 669–678. doi:10.1091/mbc.E13-09-0557.

[7] J.F. Abenza, A. Pantazopoulou, J.M. Rodríguez, A. Galindo, M.A. Peñalva, **Long-distance movement of *Aspergillus nidulans* early endosomes on microtubule tracks**, Traffic. 10 (2009) 57–75. doi:10.1111/j.1600-0854.2008.00848.x.

[8] R. Wedlich-Söldner, A. Straube, M.W. Friedrich, G. Steinberg, **A balance of KIF1A-like kinesin and dynein organizes early endosomes in the fungus *Ustilago maydis***, EMBO J. 21 (2002) 2946–2957. doi:10.1093/emboj/cdf296.

[9] J.H. Lenz, I. Schuchardt, A. Straube, G. Steinberg, **A dynein loading zone for retrograde endosome motility at microtubule plus-ends**, EMBO J. 25 (2006) 2275–2286. doi:10.1038/sj.emboj.7601119.

[10] I. Schuchardt, D. Assmann, E. Thines, C. Schuberth, G. Steinberg, **Myosin-V, Kinesin-1, and Kinesin-3 cooperate in hyphal growth of the fungus *Ustilago maydis***, Mol. Biol. Cell. 16 (2005) 5191–5201. doi:10.1091/mbc.e05-04-0272.

[11] O. Etxebeste, E.A. Espeso, **Neurons show the path: tip-to-nucleus communication in filamentous fungal development and pathogenesis**, FEMS Microbiol. Rev. 40 (2016) 610–624. doi:10.1093/femsre/fuw021.

[12] G. Steinberg, **On the move: endosomes in fungal growth and pathogenicity**, Nat. Rev. Microbiol. 5 (2007) 309–316. doi:10.1038/nrmicro1618.

[13] E. Bielska, Y. Higuchi, M. Schuster, N. Steinberg, S. Kilaru, N.J. Talbot, et al., **Long-distance endosome trafficking drives fungal effector production during plant infection**, Nat Commun. 5 (2014) 5097–14. doi:10.1038/ncomms6097.

[14] S.C. Guimaraes, M. Schuster, E. Bielska, G. Dagdas, S. Kilaru, B.R.A. Meadows, et al., **Peroxisomes, lipid droplets, and endoplasmic reticulum "hitchhike" on motile early endosomes**, J. Cell Biol. 211 (2015) 945–954. doi:10.1083/jcb.201505086.

[15] J. Salogiannis, S.L. Reck-Peterson, **Hitchhiking: A non-canonical mode of microtubule-based transport**, Trends Cell Biol. 27 (2017) 141–150. doi:10.1016/j.tcb.2016.09.005.

[16] S. Baumann, J. König, J. Koepke, M. Feldbrügge, **Endosomal transport of septin mRNA and protein indicates local translation on endosomes and is required for**

**correct septin filamentation**, EMBO Rep. 15 (2014) 94–102. doi:10.1002/embr.201338037.
[17] S. Zander, S. Baumann, S. Weidtkamp-Peters, M. Feldbrügge, **Endosomal assembly and transport of heteromeric septin complexes promote septin cytoskeleton formation**, J. Cell Sci. 129 (2016) 2778–2792. doi:10.1242/jcs.182824.
[18] Y. Higuchi, P. Ashwin, Y. Roger, G. Steinberg, **Early endosome motility spatially organizes polysome distribution**, J. Cell Biol. 204 (2014) 343–357. doi:10.1083/jcb.201307164.
[19] J.P. Latgé, ***Aspergillus fumigatus*** **and aspergillosis**, Clin. Microbiol. Rev. 12 (1999) 310–350.
[20] B. Philippe, O. Ibrahim-Granet, M.C. Prevost, M.A. Gougerot-Pocidalo, M. Sanchez Perez, A. Van der Meeren, et al., **Killing of *Aspergillus fumigatus* by alveolar macrophages Is mediated by reactive oxidant intermediates, Infection and Immunity**. 71 (2003) 3034–3042. doi:10.1128/IAI.71.6.3034-3042.2003.
[21] O. Ibrahim-Granet, B. Philippe, H. Boleti, E. Boisvieux-Ulrich, D. Grenet, M. Stern, et al., **Phagocytosis and intracellular fate of *Aspergillus fumigatus* conidia in alveolar macrophages**, Infect. Immun. 71 (2003) 891–903. doi:10.1128/iai.71.2.891-903.2003.
[22] D.W. Denning, **Invasive aspergillosis**, Clin. Infect. Dis. (1998).
[23] A. Brand, **Hyphal growth in human fungal pathogens and its role in virulence**, Int J Microbiol. 2012 (2012) 517529–11. doi:10.1155/2012/517529.
[24] M.C. Almeida, A.C. Brand, **Thigmo Responses: the fungal sense of touch**, Microbiol Spectr. 5 (2017) 487–507. doi:10.1128/microbiolspec.FUNK-0040-2016.
[25] M.A. Peñalva, J. Zhang, X. Xiang, A. Pantazopoulou, **Transport of fungal RAB11 secretory vesicles involves myosin-5, dynein/dynactin/p25, and kinesin-1 and is independent of kinesin-3**, Mol. Biol. Cell. 28 (2017) 947–961. doi:10.1091/mbc.E16-08-0566.
[26] Y. Togo, Y. Higuchi, Y. Katakura, K. Takegawa, **Early endosome motility mediates α-amylase production and cell differentiation in *Aspergillus oryzae***, Sci Rep. 7 (2017) 15757–14. doi:10.1038/s41598-017-16163-1.
[27] F. Ellett, J. Jorgensen, G.H. Frydman, C.N. Jones, D. Irimia, **Neutrophil interactions stimulate evasive hyphal branching by *Aspergillus fumigatus***, PLoS Pathog. 13 (2017) e1006154. doi:10.1371/journal.ppat.1006154.
[28] S.D. Harris, **Hyphal branching in filamentous fungi**, Dev. Biol. 451 (2019) 35–39. doi:10.1016/j.ydbio.2019.02.012.
[29] O.Y. Ponomareva, I.C. Holmen, A.J. Sperry, K.W. Eliceiri, M.C. Halloran, **Calsyntenin-1 regulates axon branching and endosomal trafficking during sensory neuron development *in vivo***, J. Neurosci. 34 (2014) 9235–9248. doi:10.1523/JNEUROSCI.0561-14.2014.
[30] D. Satoh, D. Sato, T. Tsuyama, M. Saito, H. Ohkura, M.M. Rolls, et al., **Spatial control of branching within dendritic arbors by dynein-dependent transport of Rab5-endosomes**, Nat. Cell Biol. 10 (2008) 1164–1171. doi:10.1038/ncb1776.
[31] M.J. Egan, M.A. McClintock, S.L. Reck-Peterson, **Microtubule-based transport in filamentous fungi**, Curr. Opin. Microbiol. 15 (2012) 637–645. doi:10.1016/j.mib.2012.10.003.
[32] S.D. Harris, **Branching of fungal hyphae: regulation, mechanisms and comparison with other branching systems**, Mycologia. 100 (2008) 823–832. doi:10.3852/08-177.
[33] M. Momany, N.J. Talbot, **Septins focus cellular growth for host infection by pathogenic fungi**, Front Cell Dev Biol. 5 (2017) 33. doi:10.3389/fcell.2017.00033.

[34] S.D. Harris, N.D. Read, R.W. Roberson, B. Shaw, S. Seiler, M. Plamann, et al., **Polarisome meets spitzenkörper: microscopy, genetics, and genomics converge**, Eukaryot Cell. 4 (2005) 225–229. doi:10.1128/EC.4.2.225-229.2005.

[35] M. Held, O. Kašpar, C. Edwards, D.V. Nicolau, **Intracellular mechanisms of fungal space searching in microenvironments**, Proc. Natl. Acad. Sci. U.S.A. 116 (2019) 13543–13552. doi:10.1073/pnas.1816423116.

[36] J.F. Abenza, A. Galindo, A. Pantazopoulou, C. Gil, V. de los Ríos, M.A. Peñalva, **Aspergillus RabBRab5 integrates acquisition of degradative identity with the long distance movement of early endosomes**, Mol. Biol. Cell. 21 (2010) 2756–2769. doi:10.1091/mbc.e10-02-0119.

[37] J.F. Abenza, A. Galindo, M. Pinar, A. Pantazopoulou, V. de los Ríos, M.A. Peñalva, **Endosomal maturation by Rab conversion in *Aspergillus nidulans* is coupled to dynein-mediated basipetal movement**, Mol. Biol. Cell. 23 (2012) 1889–1901. doi:10.1091/mbc.e11-11-0925.

[38] M. Hernández-González, I. Bravo-Plaza, M. Pinar, V. de los Ríos, H.N. Arst, M.A. Peñalva, **Endocytic recycling via the TGN underlies the polarized hyphal mode of life**, PLoS Genet. 14 (2018) e1007291. doi:10.1371/journal.pgen.1007291.

[39] A. Virag, M.P. Lee, H. Si, S.D. Harris, **Regulation of hyphal morphogenesis by cdc42 and rac1 homologues in *Aspergillus nidulans***, Mol. Microbiol. 66 (2007) 1579–1596. doi:10.1111/j.1365-2958.2007.06021.x.

[40] R.P. Vivek-Ananth, K. Mohanraj, M. Vandanashree, A. Jhingran, J.P. Craig, A. Samal, **Comparative systems analysis of the secretome of the opportunistic pathogen *Aspergillus fumigatus* and other Aspergillus species**, Sci Rep. 8 (2018) 6617–16. doi:10.1038/s41598-018-25016-4.

[41] S.D. Willger, S. Puttikamonkul, K.-H. Kim, J.B. Burritt, N. Grahl, L.J. Metzler, et al., **A sterol-regulatory element binding protein is required for cell polarity, hypoxia adaptation, azole drug resistance, and virulence in *Aspergillus fumigatus***, PLoS Pathog. 4 (2008) e1000200. doi:10.1371/journal.ppat.1000200.

[42] H. Li, B.M. Barker, N. Grahl, S. Puttikamonkul, J.D. Bell, K.D. Craven, et al., **The small GTPase RacA mediates intracellular reactive oxygen species production, polarized growth, and virulence in the human fungal pathogen *Aspergillus fumigatus***, Eukaryotic Cell. 10 (2011) 174–186. doi:10.1128/EC.00288-10.

[43] J.L. Slater, L. Gregson, D.W. Denning, P.A. Warn, **Pathogenicity of *Aspergillus fumigatus* mutants assessed in *Galleria mellonella* matches that in mice**, Med. Mycol. 49 Suppl 1 (2011) S107–13. doi:10.3109/13693786.2010.523852.

[44] N. Grahl, S. Puttikamonkul, J.M. Macdonald, M.P. Gamcsik, L.Y. Ngo, T.M. Hohl, et al., **In vivo hypoxia and a fungal alcohol dehydrogenase influence the pathogenesis of invasive pulmonary aspergillosis**, PLoS Pathog. 7 (2011) e1002145. doi:10.1371/journal.ppat.1002145.

[45] T.L. Orr-Weaver, J.W. Szostak, R.J. Rothstein, [14] **Genetic applications of yeast transformation with linear and gapped plasmids**, in: Recombinant DNA Part C, Elsevier, 1983: pp. 228–245. doi:10.1016/0076-6879(83)01017-4.

[46] J.W. Bok, N.P. Keller, **LaeA, a regulator of secondary metabolism in Aspergillus spp**, Eukaryot Cell. 3 (2004) 527–535. doi:10.1128/ec.3.2.527-535.2004.

[47] P. Mangeol, B. Prevo, E.J.G. Peterman, **KymographClear and KymographDirect: two tools for the automated quantitative analysis of molecular and cellular dynamics using kymographs**, Mol. Biol Cell. 27 (2016) 1948–1957. doi:10.1091/mbc.E15-06-0404.

**Supplementary Material**

Supplementary Movie 1. **Early endosomes undergo long-distance bidirectional motility the highly polarized hyphae of *Aspergillus fumigatus*.** mKate2-RabA5-labelled ealy endosomes moving relative to Histone-H1-tagGFP2-labelled nuceli. Images were acquired every 100 ms.

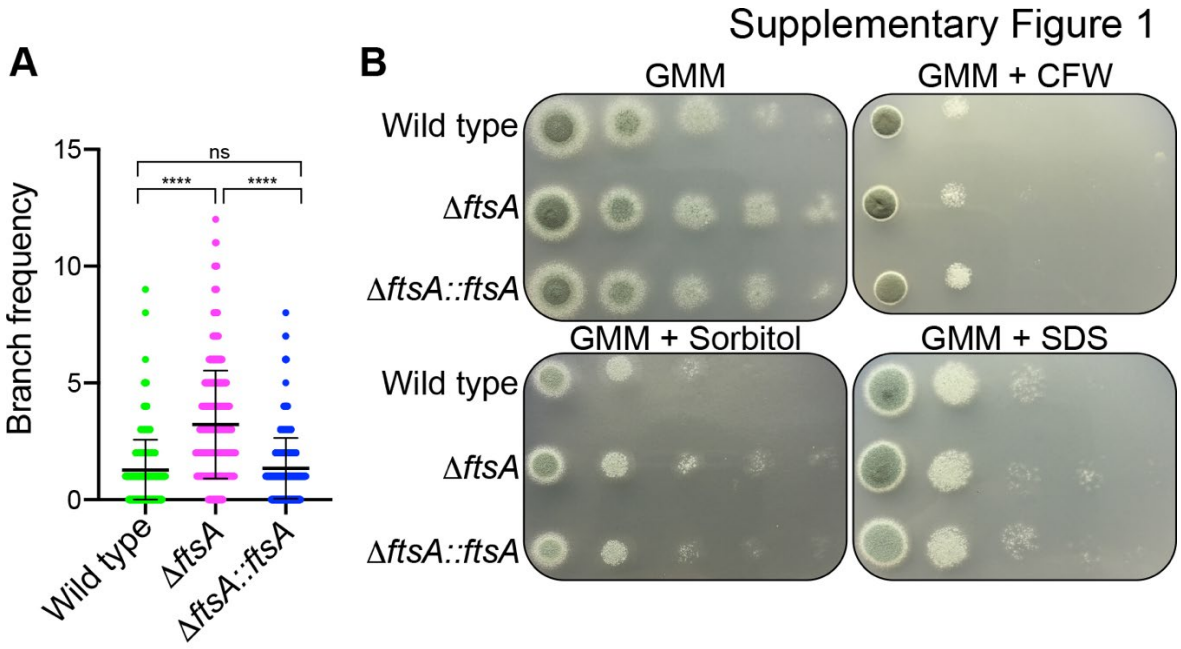


Supplementary Figure 1. **The Δ*ftsA* mutant produces more lateral branches during normal vegetative growth but shows unaltered tolerance to several cellular stressors. A** Plot showing the number of lateral branches occuring over a 400 μm region extending back from the hyphal tips (branch frequency) in wild type, Δ*ftsA* (magenta) and Δ*ftsA::ftsA*. Mean ± SD values are shown. For wild type, the mean branch frequency is 1.3 ± 1.3 (SD) and *n* = 399, for Δ*ftsA* = 3.2 ± 2.3 and *n* = 447, and for Δ*ftsA::ftsA* 1.3 ± 1.3 and *n* = 439. Asterisk indicate significance by one-way ANOVA with Tukey's multiple comparisons test (*p<0.05, **P<0.01, ***P<0.001, ****P<0.0001). **B** A ten-fold serial dilution of spores (ranging from 5 x $10^4$ to 5) from wild type, Δ*ftsA* and Δ*ftsA::ftsA* were plated onto glucose minimal media (GMM), or GMM containing 25 μg/ml calcofluor white (CFW), 90 μg/ml sodium dodecyl sulphate (SDS), or 1.2 M sorbitol. Colonies were imaged after 2 days growth at 37 ºC.

Table S1.1 Strains used in this study

| **Strain** | **Parental Strain** | **Source** |
|---|---|---|
| mKate-RabA::argB;pyrG::A.p.pyrG | AF293.6 (-pyrG, -argB) | This study |
| mKate-RabA::argB;Δfts::hyg;pyrG::A.p.pyrG | AF293.6 (-pyrG, -argB) | This study |
| mKate-RabA::argB;Δfts::hyg;fts-comp::pyrG | AF293.6 (-pyrG, -argB) | This study |
| mKate-RabA::hyg | *FGSC A1151* (-akuB, -pyrG) | This study |
| mKate-RabA::hyg;HH1-BFP::ptrA | *FGSC A1151* (-akuB, -pyrG) | This study |

Table S1.2 Plasmids used in this study and their origins.

| Cassette | Plasmid | Plasmid Source |
|---|---|---|
| *A. parasiticus pyrG* | pSD38.1 | Cramer Lab |
| *hyg* | pSD94.1 | Cramer Lab |
| *argB* | pFC331 | Momany Lab |
| *ptrA* | pSD51.1 | Cramer Lab |
| mKate2 | pME616 | Egan Lab |
| TagGFP2 | pME614 | Egan Lab |

Table S1.3. All oligonucleotide sequences used in this study.

| **Designation** | **Sequence** |
|---|---|
| A.f. mKate-RabA F1 - Upstream.F | AAC TGT TGG GAA GGG CGA TCG GTG CGG GCC TCT TTG TAA CAC TAT TGC |
| mKate-RabA F1 – Upstream.R | AAG TTC GGA GAC CAT GGC CGG CGA GCC CAA CTT |
| mKate-RabA F2 – mKate.F | TTG GGC TCG CCG GCC ATG GTC TCC GAA CTT ATT |
| mKate-RabA F2 – mKate.R | CGT TGA GTC AGA CAT GGC ACC GGC TCC AGC GCC |
| mKate-RabA F3 – ORF.F | GCT GGA GCC GGT GCC ATG TCT GAC TCA ACG AGC |
| mKate-RabA F3 – ORF.R | GAT GGC CTT CCC CAT TTA GTC TTG TAC ATA GAG |
| mKate-RabA F4 – Hyg.F | TAT GTA CAA GAC TAA ATG GGG AAG GCC ATC C |

| | |
|---|---|
| mKate-RabA F4 – Hyg.R | ATG GAG GAC TTC TTG CAG CAA CCG CAC CTG T |
| mKate-RabA F5 – Downstream.F | CAG GTG CGG TTG CTG CAA GAA GTC CTC CAT AGT |
| mKate-RabA F5 – Downstream.R | TTC ACA CAG GAA ACA GCT ATG ACC ATG ATT AGA GGA CGT GGC GGT CGG |
| mKate-RabA F1 – Upstream (No vec).F | TCT TTG TAA CAC TAT TGC |
| mKate-RabA F5 – Downstream (No vec).R | AGA GGA CGT GGC GGT CGG |
| mKate-RabA Conf.F | TGG CGC TCA TAG TGA TTG GA |
| mKate-RabA Conf.R | CCG TGT GCA CTT CGC TTT AT |
| | |
| FTS KO F1 – Upstream.F | AAC TGT TGG GAA GGG CGA TCG GTG CGG GCC TAT GCT GAT ATT GAC AAC AGC GTT CAG |
| FTS KO F1 – Upstream.R | ACA CCC AAT ACG CCG TGC CAC CAC CGT TCA AGG AGA G |
| FTS KO F2 – Hyg.F | TGA ACG GTG GTG GCA CGG CGT ATT GGG TGT TAC GGA G |
| FTS KO F2 – Hyg.R | CTG TAT ACA TCG GCA ATG GGG AAG GCC ATC CAG |
| FTS KO F3 – Downstream.F | ATG GCC TTC CCC ATT GCC GAT GTA TAC AGT ACC TGA TGG |
| FTS KO F3 – Downstream.R | TTC ACA CAG GAA ACA GCT ATG ACC ATG ATT TCA TCA CCC TCC AAC ATT TCG TCC |
| FTS KO Conf.F | AGC GAA GTA TGA GGT TGA GTC TGG |
| FTS KO Conf.R | ACC AGC GTA GTA TCA TGT CAG AGG |
| | |
| FTS Comp F1 – Upstream.F | AAC TGT TGG GAA GGG CGA TCG GTG CGG GCC GCT CGA CCT TCC GAC CAC G |
| FTS Comp F1 – Upstream.R | AAG GGT GAT GTC GAC GGT ACT ATA CCT GTA ACT ATT GTG CTT GG |
| FTS Comp F2 – PyrG.F | TAC AGG TAT AGT ACC GTC GAC ATC ACC CTT ACC CAA AC |
| FTS Comp F2 – PyrG.R | CTG TAT ACA TCG GCA GGA TCC TAT GGA TCT CAG AAC AAT ATA CCA G |
| FTS Comp F3 – Downstream.F | AGA TCC ATA GGA TCC TGC CGA TGT ATA CAG TAC CTG AT |
| FTS Comp F3 – Downstream.R | TTC ACA CAG GAA ACA GCT ATG ACC ATG ATT CCC ACA TTG GTT TCC AGT ATG TCT AG |
| FTS Comp1 F1 – Upstream (No vec).F | CGC TCG ACC TTC CGA CCA C |
| FTS Comp1 – Downstream (No vec).R | CCC ACA TTG GTT TCC AGT ATG TCT AGC |

| | |
|---|---|
| FTS ORF Conf.F | AGT GCG TCA TGC AGT G |
| FTS ORF Conf.R | CTC CTT GAT CGA AGC CAA C |
| | |
| HH1-GFP F1 – ORF Flank.F | AAC TGT TGG GAA GGG CGA TCG GTG CGG GCC TTA ATC ACG CTG TTT TCG |
| HH1-GFP F1 – ORF Flank.R | GCC TGC ACC AGC TCC CGC CTC GCT CTT CTC AGC |
| HH1-GFP F2 – GFP.F | GAG AAG AGC GAG GCG GGA GCT GGT GCA GGC GCT |
| HH1-GFP F2 – GFP.R | CTT CAG CGA TGA CAT TTA GCG AGA GCC TGT GGA |
| HH1-GFP F3 – 3'UTR.F | ACA GGC TCT CGC TAA ATG TCA TCG CTG AAG TCG |
| HH1-GFP F3 – 3'UTR.F | GTC TGT CAG ATC CCC TCT CGC ATG ACT GAA GTA |
| HH1-GFP F4 – PtrA.F | TTC AGT CAT GCG AGA GGG GAT CTG ACA GAC G |
| HH1-GFP F4 – PtrA.R | GCA AGC AAG GGA CAT CTA TCA TGG GGT GAC G |
| HH1-GFP F5 – Downstream.F | GTC ACC CCA TGA TAG ATG TCC CTT GCT TGC CG |
| HH1-GFP F5 – Downstream.R | TTC ACA CAG GAA ACA GCT ATG ACC ATG ATT TGA TTC AAG ACA GTC GA |
| HH1-GFP F1 – ORF Flank (No vec).F | TTA ATC ACG CTG TTT TCG |
| HH1-GFP F5 – Downstream (No vec).R | TGA TTC AAG ACA GTC GA |